

ORIGINAL ARTICLE

Feeding currents facilitate a mixotrophic way of life

Lasse T Nielsen and Thomas Kiørboe

Centre for Ocean Life, National Institute of Aquatic Resources, Technical University of Denmark, Charlottenlund, Denmark

Mixotrophy is common, if not dominant, among eukaryotic flagellates, and these organisms have to both acquire inorganic nutrients and capture particulate food. Diffusion limitation favors small cell size for nutrient acquisition, whereas large cell size facilitates prey interception because of viscosity, and hence intermediately sized mixotrophic dinoflagellates are simultaneously constrained by diffusion and viscosity. Advection may help relax both constraints. We use high-speed video microscopy to describe prey interception and capture, and micro particle image velocimetry (micro-PIV) to quantify the flow fields produced by free-swimming dinoflagellates. We provide the first complete flow fields of free-swimming interception feeders, and demonstrate the use of feeding currents. These are directed toward the prey capture area, the position varying between the seven dinoflagellate species studied, and we argue that this efficiently allows the grazer to approach small-sized prey despite viscosity. Measured flow fields predict the magnitude of observed clearance rates. The fluid deformation created by swimming dinoflagellates may be detected by evasive prey, but the magnitude of flow deformation in the feeding current varies widely between species and depends on the position of the transverse flagellum. We also use the near-cell flow fields to calculate nutrient transport to swimming cells and find that feeding currents may enhance nutrient uptake by $\approx 75\%$ compared with that by diffusion alone. We argue that all phagotrophic microorganisms must have developed adaptations to counter viscosity in order to allow prey interception, and conclude that the flow fields created by the beating flagella in dinoflagellates are key to the success of these mixotrophic organisms.

The ISME Journal (2015) 9, 2117–2127; doi:10.1038/ismej.2015.27; published online 17 February 2015

Introduction

Many or most eukaryotic flagellates are in principle mixotrophic, that is, they photosynthesize and take up food simultaneously (Flynn *et al.*, 2013). One implication of this is that they need to be able to both harvest dissolved inorganic nutrients and intercept and capture particulate prey. Nutrient uptake in unicellular organisms is typically constrained by the diffusive delivery of nutrients to the cell surface, and is much more efficient for small than for large cells (Munk and Riley, 1952; Fiksen *et al.*, 2013). Conversely, prey interception is constrained by viscosity for small cells operating at low Reynolds numbers because the viscous boundary layer surrounding the predator may push away the prey as it is approached (Kiørboe, 2011). Purely autotrophic organisms are, therefore, typically very small (for example, cyanobacteria), and purely heterotrophic organisms typically larger, with the mixotrophic strategy occurring mainly in intermediately sized ($\approx 5\text{--}100\ \mu\text{m}$) organisms (Stoecker,

1998) that are thus constrained both by viscosity and diffusion.

Dinoflagellates are one of the most abundant and ecologically important groups of aquatic flagellates. Most of them are either heterotrophic or mixotrophic (Stoecker, 1999). They are generally $10\text{--}100\ \mu\text{m}$ long, swim at $2\text{--}20$ body lengths s^{-1} , and hence operate at Reynolds numbers of $10^{-4}\text{--}10^{-1}$. Thus, dinoflagellates are constrained by both diffusion and viscosity but have nevertheless evolved into a diverse and hugely successful group. What has ensured this success?

Swimming will increase nutrient uptake by renewing nutrient-replete water around the cell, and swimming or feeding currents are often also required to encounter prey. The enhancement of nutrient delivery and the rate of prey encounter and prey capture success may, however, depend on the flow field that the flagellate generates (Langlois *et al.*, 2009). The advective enhancement of nutrients because of swimming/feeding currents is quantified by the Sherwood number, with $Sh=1$ for no enhancement relative to pure diffusion (Karp-Boss *et al.*, 1996). For an organism moved by a body force (such as gravity), Sherwood numbers are close to unity for the Reynolds numbers considered here, whereas it is higher for a self-propelled organism, as suggested by theoretical models based on idealized flows (Magar *et al.*, 2003; Magar and Pedley, 2005;

Correspondence: LT Nielsen, Centre for Ocean Life, National Institute of Aquatic Resources, Technical University of Denmark, Kavalergården 5, Charlottenlund 2920, Denmark.
E-mail: ltor@aqu.dtu.dk

Received 29 December 2014; accepted 8 January 2015; published online 17 February 2015

Langlois *et al.*, 2009; Bearon and Magar, 2010). Similarly, prey encounter by direct interception depends on the flow field generated by the flagellate and is higher the closer the streamlines come to the capture region on the flagellate (Langlois *et al.*, 2009). Interception feeding has been suggested as a common prey encounter mechanism in flagellates (Fenchel, 1982, 1984; Christensen-Dalsgaard and Fenchel, 2003), but feeding flows of free-swimming forms have not been described in any detail. Finally, many of the potential prey of dinoflagellates are evasive, that is, they can perceive the flow disturbance generated by the approaching flagellate, and escape (see, for example, Jakobsen, 2001). Specifically, plankton organisms may respond to fluid deformation when it exceeds a certain threshold that typically is in the range of $1\text{--}10\text{ s}^{-1}$ (Kjørboe and Visser, 1999; Kjørboe *et al.*, 1999; Jakobsen, 2001, 2002; Fenchel and Hansen, 2006). Thus, overall, there are tradeoffs between rapid swimming to enhance nutrient uptake and prey encounter versus the resulting elevated risk of eliciting prey escape responses, and these tradeoffs may depend strongly on the flow and deformation fields generated by the dinoflagellate.

Most dinoflagellates have two distinct flagella, one trailing after the cell as it swims, termed the longitudinal flagellum, and one encircling the cell, termed the transverse flagellum. The transverse flagellum and the distal end of the longitudinal flagellum are typically situated in grooves on the outside of the cell (termed the cingulum and sulcus, respectively). Combined, the two flagella propel the cell forward in a helical path (Fenchel, 2001). The position of the transverse flagellum varies between species; it is typically located equatorially, but several species have it positioned more anteriorly (Figure 1). The different flagellar arrangements likely create different flows in the near field region of the cell, with possible implications for nutrient transport and perception and capture of prey. All dinoflagellates have but a single point of prey ingestion; direct engulfment takes place only through a single non-permanent cytostome, typically located in the sulcus, and peduncles also occupy a fixed position, also typically originating from the sulcus (see Figure 1) (Hansen and Calado, 1999). It is unknown how dinoflagellates ensure that prey arrives to this particular region. It is also unknown to what extent the flagella are involved in, or mediate, prey capture.

In this study we describe for the first time the flow fields generated by seven species of dinoflagellates with different flagellar arrangements in order to assess all the three aspects of nutrient acquisition considered above. Only recently it has become possible to measure the flow fields around microorganisms, and such observations exist only for a few organisms and were collected mainly in the context of nutrient acquisition and fluid dynamics of swimming (Drescher *et al.*, 2010, 2011; Kjørboe

et al., 2014; Goldstein, 2015). We use micro particle image velocimetry (micro-PIV) to visualize the flow and high-speed video microscopy to describe prey encounter and prey capture. We demonstrate that feeding flows are sufficient to account for observed clearance rates and that the flows generated differ between species and likely represent adaptations to feeding on evasive and nonevasive prey. Finally, the flows imply significantly elevated nutrient uptake rates relative to that because of pure diffusion.

Materials and methods

Cultures and laboratory conditions

We studied seven species of mixotrophic and heterotrophic dinoflagellates (Figure 1 and Table 1). Two of these species are peduncle feeders (*Amphidinium longum* and *Dinophysis acuta*), whereas the rest engulf particles directly. All experimental organisms were taken from our culture collection. The cultures were grown in B1-medium with a salinity of 32 at 20°C . Most of the mixotrophic species grew photoautotrophically at $\approx 100\ \mu\text{mol photons m}^{-2}\text{ s}^{-1}$. *D. acuta* is an obligate mixotroph and was fed the mixotrophic ciliate *Mesodinium rubrum* that, in turn, was fed the cryptophyte *Teleaulax amphioxeia* (Park *et al.*, 2006). The heterotrophic dinoflagellates were fed weekly with *Rhodomonas salina* and presented with only low light level ($\approx 5\ \mu\text{mol photons m}^{-2}\text{ s}^{-1}$).

Experimental setup

Observations of swimming and feeding dinoflagellates were made using an Olympus IX71 inverted microscope (Olympus, Ballerup, Denmark) equipped with $4\text{--}100\times$ DIC objectives, two build-in magnifying lenses ($1\text{--}1.6\times$ and $1\text{--}2\times$) and a Phantom V210 high-speed ($10^2\text{--}10^3\text{ frames s}^{-1}$), high-resolution (1280×800 pixels) video camera capable of post-triggering (Vision Research, Wayne, NJ, USA). Fields of view ranged from $0.64\text{ mm}\times 0.40\text{ mm}$ when applying the $40\times$ objective to $0.26\text{ mm}\times 0.16\text{ mm}$ when applying the $100\times$ objective. The organisms swam in $10\text{ mm}\times 10\text{ mm}$ chambers 0.5 mm high. These were produced using several layers of cover slip glass mounted on a microscope slide with silicone grease. The microscope was focused in the middle of this chamber, ensuring that wall effects were negligible. Cell concentrations were never higher than one to few cells per field of view, and most often much less. The whole setup was placed in an air-conditioned room set to 16°C . Swimming speed, U , was calculated from the position of the cell relative to the camera in consecutive frames as:

$$U = \sqrt{\Delta x^2 + \Delta y^2} \times \frac{fps}{\Delta f}$$

where Δx and Δy are the changes in x and y in μm between the two frames, fps is the frame rate of the

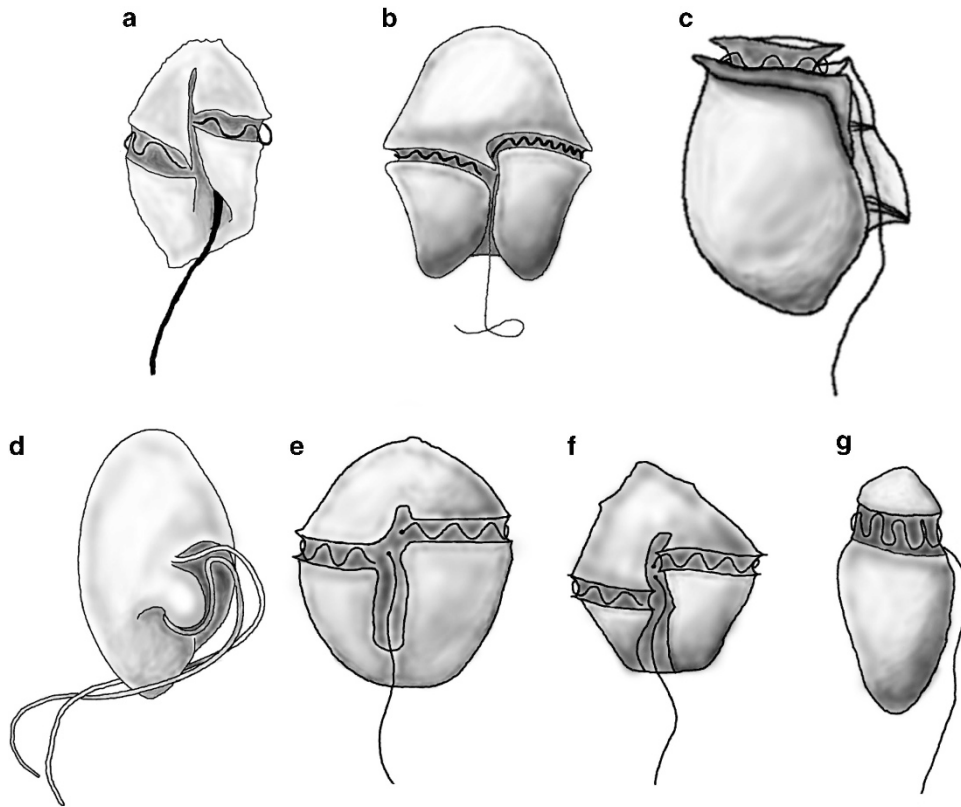


Figure 1 Schematic drawings of the experimental organisms. *Gyrodinium dominans* (a); *Akashiwo sanguinea* (b); *Dinophysis acuta* (c); *Oxyrrhis marina* (d); *Protoceratium reticulatum* (e); *Lingulodinium polyedrum* (f); *Amphidinium longum* (g). (a, b, e, f) all have the transverse flagellum situated equatorially, like the majority of dinoflagellates. (c, g) have it positioned more anteriorly. (d) Does not have a distinct transverse flagellum.

Table 1 Studied dinoflagellate species, and characteristics of their morphology, trophic mode and swimming

Species name	Length (μm)	Width (μm)	Transverse flagellum ^a	Trophic mode	Swim speed ($\mu\text{m s}^{-1}$)	Re^b
<i>Akashiwo sanguinea</i>	73 ± 15	46 ± 3	Equatorial	Mixotrophic	45 ± 18	1.3×10^{-3}
<i>Amphidinium longum</i>	29 ± 3	17 ± 4	Anterior	Heterotrophic	84 ± 47	9.6×10^{-4}
<i>Dinophysis acuta</i>	79 ± 5	54 ± 5	Anterior	Mixotrophic	104 ± 36	3.5×10^{-3}
<i>Gyrodinium dominans</i>	24 ± 3	14 ± 2	Equatorial	Heterotrophic	259 ± 57	2.5×10^{-3}
<i>Lingulodinium polyedrum</i>	36 ± 5	32 ± 3	Equatorial	Mixotrophic	105 ± 52	1.8×10^{-3}
<i>Oxyrrhis marina</i>	30 ± 2	18 ± 1	Other	Heterotrophic	256 ± 10	3.1×10^{-3}
<i>Protoceratium reticulatum</i>	40 ± 6	36 ± 7	Equatorial	Mixotrophic	145 ± 30	2.7×10^{-3}

^aDenotes position of the transverse flagellum. *Oxyrrhis marina* does not have a distinct transverse flagellum.

^bReynolds number calculated as $Re = u \times a / \nu$, where u is the swimming speed, a the average cell radius and ν a kinematic viscosity of $10^{-2} \text{ cm}^2 \text{ s}^{-1}$.

particular video in frames s^{-1} and Δf is the number of frames between the two selected frames.

Prey capture observations

Prey capture was observed in *A. longum*, *Gyrodinium dominans* and *Oxyrrhis marina* offered the $6 \mu\text{m}$ -sized flagellate *R. salina* (Figure 2 and Supplementary Movie S3). We monitored swimming and feeding dinoflagellates and simply captured sequences where prey capture happened in the field of view and in focus. Numerous (>20) prey capture events were observed at low magnification ($\times 40$ to $\times 200$) for each of the species. Where possible, these

were supported by high-magnification ($\times 400$ to $\times 2000$) recordings. For *O. marina*, 18 such high-magnification sequences were recorded. For *A. longum* and *G. dominans*, only a few were recorded because of the limitations set by the combination of the limited field of view, the more dilute cultures and the rarity of food capture events.

Dinophysis acuta feeds solely on *M. rubrum*, but despite hours of observation we never managed to record a capture event similar to that tentatively described for *D. acuminata* before (Hansen *et al.*, 2013). The remaining species grew photoautotrophically in our cultures, and we did not attempt to observe prey capture.

Flow visualization

Flow fields generated by feeding and swimming dinoflagellates were visualized and quantified using micro-PIV (Figure 3). We used the same swimming chambers as above but seeded the water with $0.5\ \mu\text{m}$ neutrally buoyant polymer spheres (Nanospheres, Duke Scientific Corp., Palo Alto, CA, USA). Rather than using a laser sheet to define the observation plane as in traditional PIV, this plane was here simply defined by the focal depth of the objective. The focal depth is not an exact quantity, but at the magnifications used here, the focal depth is one to few μm (Berek, 1927). Only videos where the experimental organism was in focus and moved in the focal plane were used. Organisms were masked using ImageJ 1.46r (<http://imagej.nih.gov/ij/>) before analysis of the flow fields. Video sequences were analyzed using DaVis PIV software 8.0.6 (Lavisoin GmbH, Goettingen, Germany) to quantify the water flow generated by the swimming dinoflagellates. This software also allows us to compute fluid deformation fields. The relevant property in the

context of prey signal perception is the maximum strain rate (Kjørboe and Visser, 1999). For comparisons between species, we contoured the $3\ \text{s}^{-1}$ value. This is also the threshold strain rate that will elicit escape reactions in *M. rubrum*, the prey of *Dinophysis* spp.

In order to quantify and visualize the flow relative to the swimming organism (rather than the camera), the swimming velocity of the organism was subtracted from the flow field. This was achieved within the DaVis software. These flow fields were used to calculate the potential clearance rates and the flux of inorganic nutrients as described below.

Clearance rates

Potential clearance rates were calculated for the two heterotrophic dinoflagellates *G. dominans* and *O. marina* based on the observed flow fields, and the observation that both species capture and ingest prey items only in the sulcus–cingulum intersection (point of capture). The clearance rate was calculated as the flow through a cross-sectional area next to the

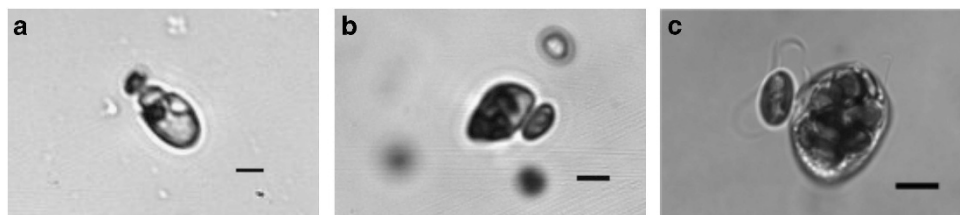


Figure 2 Stills from high-speed videos of prey capture in *Amphidinium longum* (a), *Gyrodinium dominans* (b) and *Oxyrrhis marina* (c). *A. longum* captures the prey at its own anterior end, whereas the other two do it laterally near the origin of the two flagella.

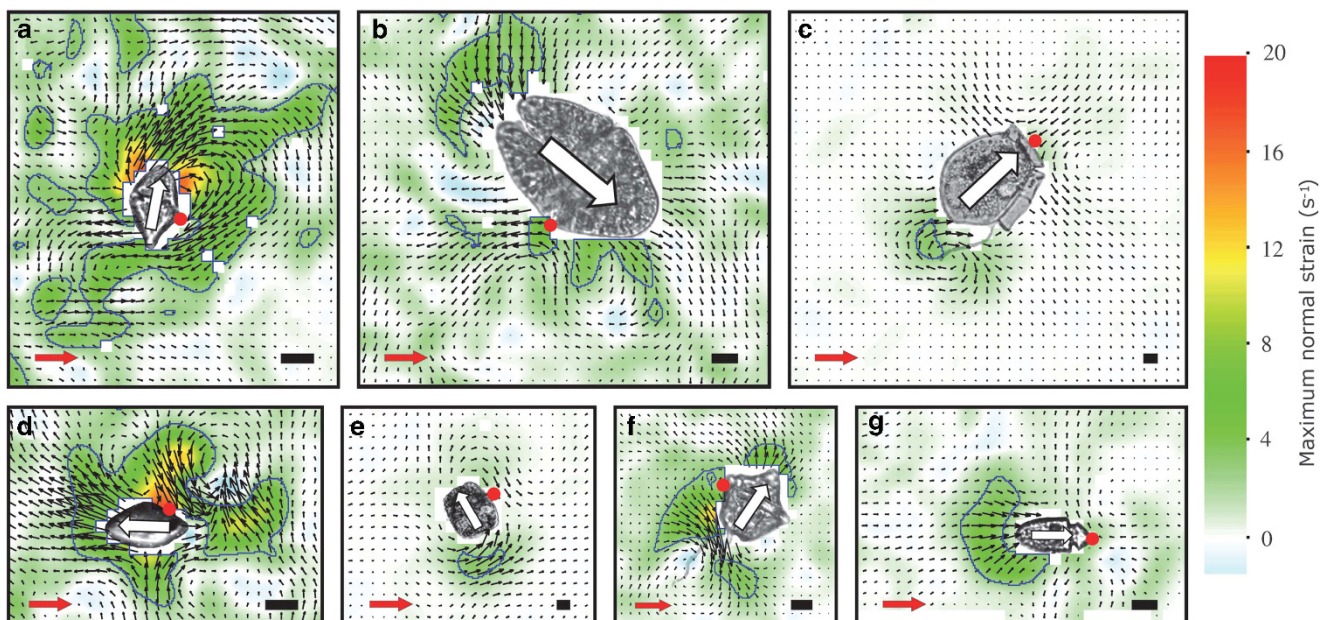


Figure 3 Flow and shear fields of the seven species of dinoflagellates. *Gyrodinium dominans* (a); *Akashiwo sanguinea* (b); *Dinophysis acuta* (c); *Oxyrrhis marina* (d); *Protoceratium reticulatum* (e); *Lingulodinium polyedrum* (f); *Amphidinium longum* (g). Organisms have been cropped in from the original videos. White arrows indicate the swimming direction. Black length scales are $10\ \mu\text{m}$. Black vectors show the flow field, and the red arrow represents a $100\ \mu\text{m}\ \text{s}^{-1}$ scale. The color scheme denotes the fluid deformation, and the blue contour line shows the $3\ \text{s}^{-1}$ threshold value (see text). The red dots mark the point of prey capture, as either observed here or from the literature. See text for interpretation.

point of capture, with the size of this area dependent only upon the prey size. The cross-sectional feeding area was calculated slightly differently for the two species (Figure 4). Adopting an anterior or posterior view, for *G. dominans*, it was calculated as a circle centered in the dinoflagellate's point of capture and with a radius equal to one prey radius (Figure 4a). The overlapping area of the circle that represented the dinoflagellate was subtracted. *O. marina* has a $\approx 5 \mu\text{m}$ wide ventral bulge believed to be the capture site. Again from an anterior or posterior view, an area of $5 \mu\text{m} \times$ the prey radius was thus added to the cross-sectional area otherwise calculated as for *G. dominans* (Figure 4b).

Flow velocities through the feeding area were extracted using the DaVis software. For all prey sizes, the potential clearance rate was calculated as the cross-sectional area of the feeding current multiplied by the average flow velocity through this area (Figure 5). Four independent flow fields were analyzed from each of three videos ($n = 12$) for both species.

For comparison, literature values of maximum clearance rates were compiled for both species. For *O. marina*, data comprised sources collected by Roberts *et al.* (2011), and for *G. dominans* those collected by Lee *et al.* (2014) supplemented by the study of Yoo *et al.* (2010). Where clearance rates were not explicitly given, these were calculated as the initial slope of ingestion vs prey concentration curves. For each data set, the growth rate at food-replete conditions had to be at least 50% of the maximum growth rate reported across all data sets, else the clearance data were excluded. This was done to avoid false low clearance rates because of escaping prey or negative prey selection.

Nutrient uptake and Sherwood number

Flow fields relative to the organism also provided the basis for calculations of nutrient transport to

swimming *D. acuta* cells. This particular species was chosen for its approximately rotational symmetrical and stationary flow field that allows for conversion from two-dimensional observations to a three-dimensional approximation. A similar flow field was found in *A. longum* but this species is purely heterotrophic, and presumably does not take up inorganic nutrients. The asymmetric two-dimensional flow fields of the remaining species could not satisfactorily be converted to the three-dimensional flow fields needed for flux calculations.

First, the best axis of symmetry was identified for each frame, and the two halves were averaged. The observed flow fields were not entirely divergence free, as assumed by our calculations. Thus, a divergence-free flow field was matched to best fit the observed average flow field using a least squares fitting approach in MATLAB v. R2013a (MathWorks, Natick, MA, USA; Figure 6b). An ellipse was fitted to best represent the outline of the dinoflagellate. The steady-state concentration field was calculated using Comsol v. 4.4 (Comsol Inc., Burlington, MA, USA) and by assuming a constant concentration in the far field, a concentration of zero at the dinoflagellate surface and a specific diffusion coefficient, $D = 10^{-9} \text{m}^2 \text{s}^{-1}$. The integrated flux was then calculated, both for the observed flow field and for the case of no fluid flow, and the Sherwood number was computed as the ratio of the two integrated fluxes (that is, the enhancement of nutrient transport due to advections). The calculation was repeated for 30 individual video frames.

Results

Flagellar arrangements and swimming speeds

The studied dinoflagellates were separated into three groups based on the position of the transverse flagellum (Figure 1 and Table 1). One type has the transverse flagellum positioned approximately

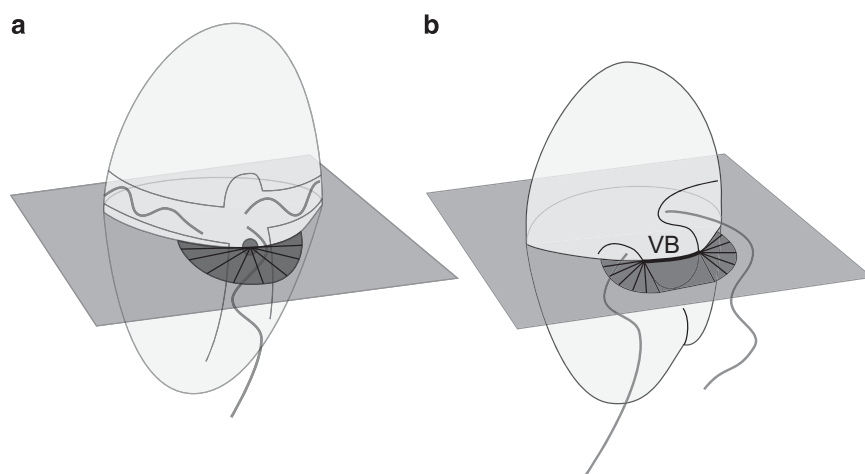


Figure 4 Schematic figure of the cross-sectional area (dark shaded) of the feeding current in *Gyrodinium dominans* (a) and *Oxyrrhis marina* (b). In (a), the area is a circle ($r =$ prey radius) minus the area of the circle that is the dinoflagellate predator. The dark gray dot indicates the point of capture. In (b), the area is a rectangle ($5 \mu\text{m} \times$ prey radius) outside the ventral bulge (VB) plus a circle sector ($r =$ prey radius) on either side. Prey is caught all along the width of the ventral bulge.

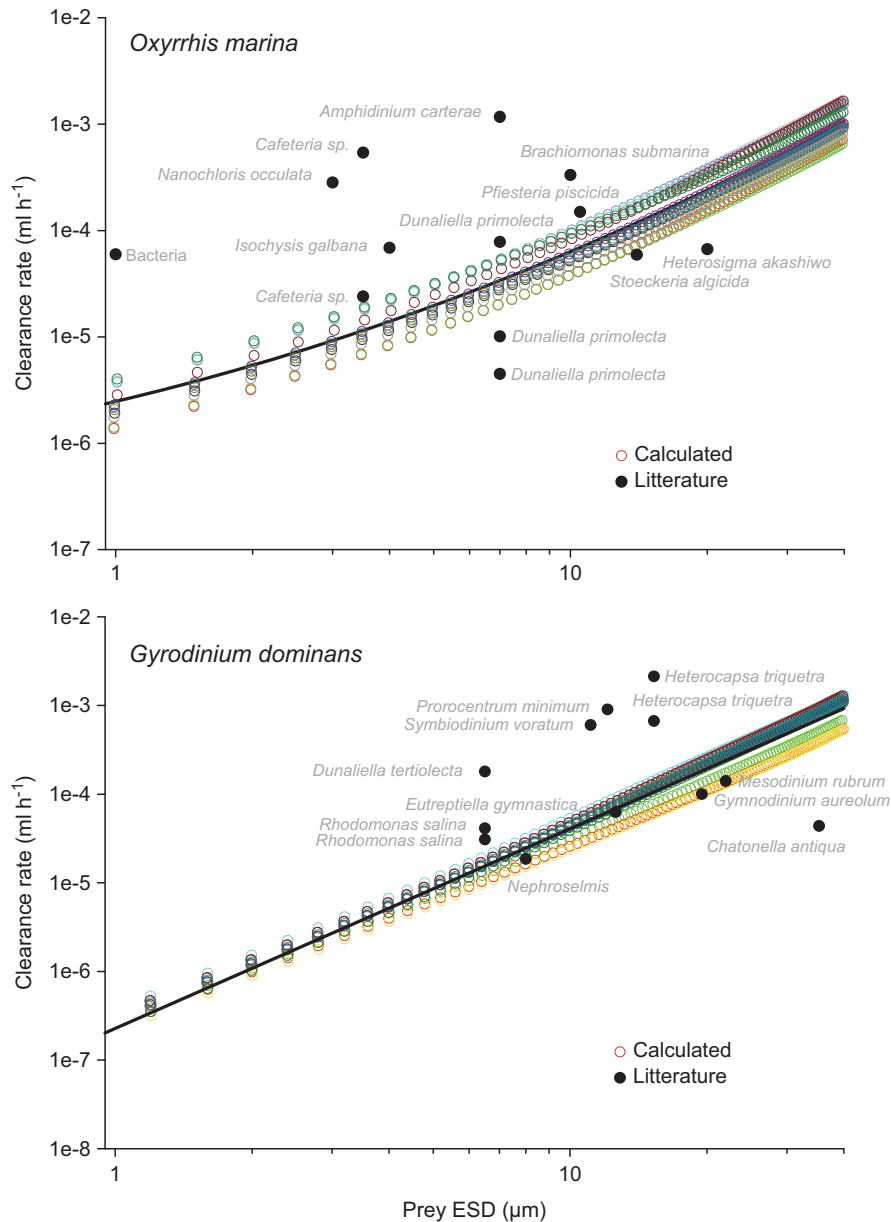


Figure 5 Clearance rates of *Oxyrrhis marina* (top) and *Gyrodinium dominans* (bottom) as a function of prey size. Colored circles show our calculated values for each of the 12 replicate frames. The solid black line is a least squares linear regression. Black dots are literature values.

equatorially. This resembles the most common dinoflagellate morphology. A second group has the transverse flagellum positioned anteriorly, whereas the evolutionary primitive *O. marina* does not have a distinct transverse flagellum, and fell in its own group. The dinoflagellates ranged in length from ~ 25 to $80 \mu\text{m}$, and swam at speeds between 45 and $260 \mu\text{m s}^{-1}$, corresponding to 0.6 – 11 body lengths s^{-1} . Reynolds numbers of the swimming dinoflagellates were in the range of 1.0×10^{-3} – 3.5×10^{-3} .

Prey capture

High-speed videography of prey capture events revealed several striking and surprising features

of the prey capture process (Figure 2 and Supplementary Movie S1). First and foremost, none of the observed dinoflagellates pushed the prey away when approaching, as otherwise speculated.

A. longum made first contact with the prey at its own anterior (frontal) end, that is, simply swam up to the prey (Figure 2 and Supplementary Movie S1). Prey cells were not pushed away, but rather pulled slightly toward the approaching predator. *A. longum* then connected to the prey with a peduncle within 4–6 s from the first cell–cell contact. No other means of attachment (for example, capture filament) were observed, and the otherwise rather oblivious prey, *R. salina*, was on a few occasions seen to perform successful escape jumps during this interval.

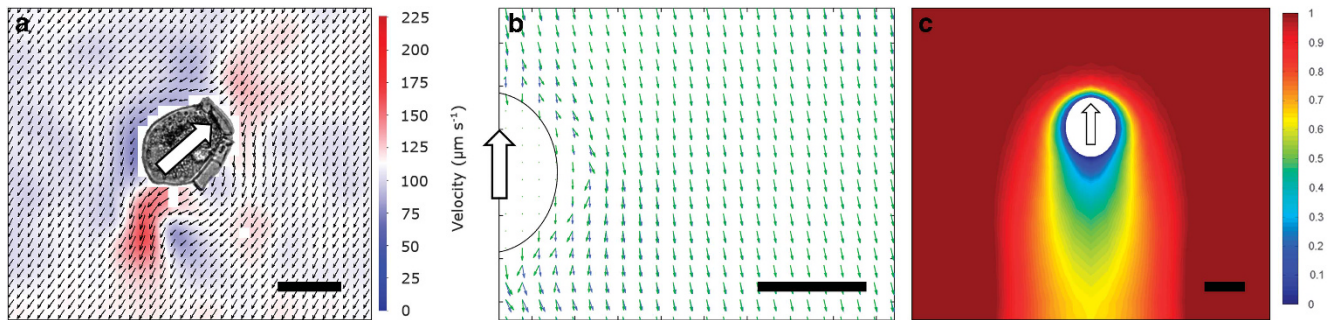


Figure 6 *Dinophysis acuta*, a single video frame. Flow relative to the organism (a), observed (blue) and optimized (green) flow fields used for calculations of diffusion (b) and the resulting concentration field (c). Scale bars are $50\ \mu\text{m}$ and white arrows show the swimming direction. The swimming velocity of *D. acuta* was $113\ \mu\text{m s}^{-1}$, corresponding to the white color in (a). Blue colors thus represent water that to some extent moves with the dinoflagellate, whereas red colors represent water that moves faster (relative to the organism) than prescribed by the swimming speed of the organism alone (that is, actively pulled opposite the swimming direction). The observed flow field (blue) in (b) is the average of the left and right side of the axis of symmetry. The concentration field (c) shows a steep decline in nutrient concentration in front and to the sides of the cell. The color scheme is relative. The Sherwood number computed using the flow field was 1.75 ± 0.06 , denoting a 75% increase in nutrient uptake because of swimming.

This happened only, however, after extensive cell–cell physical contact, and was not a reaction to fluid disturbances.

G. dominans never swam into a prey cell with its anterior end. Instead, it always made first contact with the equatorial parts of its own cell (Figure 2 and Supplementary Movie S1). This suggests a flow toward this particular area of the cell. After first contact, *G. dominans* circled around the prey and bumped into it several times with its own equatorial part. After a few such close contacts, the actual prey capture was facilitated by the deployment of a capture filament, after which *G. dominans* swam away with the prey attached at the end of a ca. $30\ \mu\text{m}$ long filament. Ingestion was through whole cell phagocytosis.

O. marina, like *G. dominans*, never swam into a prey cell with its anterior end. It too managed always to meet the prey with the area of prey capture (the ventral bulge, near the origin of the two flagella). First contact was immediately followed by an upfolding of the trailing flagellum such that the flagellum encircled the prey item. This ensured that *O. marina* kept a close contact with the prey item as it circled around it several times. We interpret the upfolding of the trailing flagellum as a mechanism of prey manipulation, seemingly in order to achieve correct prey alignment before attachment, and possibly to keep the prey from escaping. No evidence of a capture filament was found; instead *O. marina* seemed to simply attach to the prey at the ventral bulge after a few seconds of prey manipulation. Ingestion was through whole cell phagocytosis.

Flow fields and potential clearance rates

In all dinoflagellates, the trailing flagellum produced short-lived, counter-rotating flow structures behind the swimming cell. This part of the flow field was thus highly fluctuating and in synchrony with the beating of the flagellum (Figure 3 and Supplementary Movies S2 and S3). In contrast, the transverse

flagellum created distinctly different flow fields depending on its position on the cell: dinoflagellates with the transverse flagellum positioned anteriorly (*A. longum* and *D. acuta*) had near radial symmetric flow fields, with water in front of the cell moving toward it and out to the sides (Figures 3c and g and Supplementary Movies S2 and S3). The flow velocities in this part of the flow field were almost constant, and the anterior incoming flow of water intercepts the cell at the position of prey capture in *A. longum* and presumably also *D. acuta*.

In contrast, dinoflagellates with the transverse flagellum positioned equatorially (*Akashiwo sanguinea*, *G. dominans*, *Lingulodinium polyedrum* and *Protoceratium reticulatum*) all pushed water in front of the swimming cell, and had a flow toward the transverse flagellum. This flow was asymmetric and by far the strongest on the side of the cell where the trailing flagellum is positioned, consequently making the flow directed toward the cingular–sulcus intersection (Figure 3 and Supplementary Movies S2 and S3). This is also the region of prey capture and phagocytosis, effectively making it a feeding current. In the two-dimensional observations, these asymmetric flow fields appeared highly fluctuating, as the dinoflagellate cells rotate around their own length axis when swimming. The feeding current was thus most pronounced when the cells were oriented with one of the two lateral sides toward the camera, and the focus depth matched the primary plane of the flow. The flow field of *O. marina* resembled that of dinoflagellates with an equatorial transverse flagellum. Thus, in all species, flows are created that bring prey particles to the capture position on the cell, or at least prevent cells from being pushed away. These flows can consequently be considered feeding currents.

Potential clearance rates computed from the observed flow fields of *G. dominans* increased with prey size and ranged from 2×10^{-7} to $5 \times 10^{-4}\ \text{ml h}^{-1}$ for prey sizes 1 to $30\ \mu\text{m}$ (Figure 5). For *O. marina*, the corresponding values were 2×10^{-6} to

$5 \times 10^{-4} \text{ ml h}^{-1}$ (Figure 5). For comparison, clearance rates reported in the literature are also plotted and observed and predicted clearance rate are of similar order of magnitude, at least for the larger prey cells.

Deformation fields

The different dinoflagellate species created highly different intensities of fluid deformation (Figure 3 and Supplementary Movies S2 and S3). Both species with the transverse flagellum positioned anteriorly produced relatively little deformation, and in the area in front of the cell, where prey is intercepted, the deformation never exceeded the threshold of 3 s^{-1} . *A. sanguinea* and *P. reticulatum* both swam slowly and created very little fluid deformation. Only small areas in front of the cells, very near the transverse flagella and in the immediate wake of the cells had values of deformation exceeding 3 s^{-1} . *L. polyedrum* swam slightly faster, and caused significantly more fluid deformation, especially in the feeding current directed toward the sulcus–cingulum junction. *G. dominans* and *O. marina* were the fastest swimmers and both created large areas of high fluid deformation, particularly in front of the cell and in the flow directed toward the sulcus–cingulum junction.

Concentration fields and nutrient fluxes

The flow field relative to the swimming *D. acuta* was quite stationary and nearly rotational symmetric (Figure 6a and Supplementary Movie S4). Some fitting was needed to achieve a divergence-free flow field, especially very near the cell (Figure 6b). The computed concentration field around *D. acuta* showed steep gradients in front and to the sides of the cell (Figure 6c). The Sherwood number was found to be 1.75 ± 0.06 (mean \pm s.d., $n = 30$), corresponding to an increase in nutrient uptake due to advection (swimming and feeding currents) by 75% relative to that due to pure diffusion.

Discussion

Prey capture and interception feeding

Our observations suggest that all dinoflagellates produce feeding currents that both allow direct interception of prey particles and lead to increased prey encounter rates. Rather than pushing the prey away as they approach, they make use of small-scale flow structures to position the prey near a specific area of their own cell. *O. marina* and the dinoflagellates with an equatorial transverse flagellum do, as hypothesized, push water in front as they swim. This would mean reduced prey encounter rates, but these dinoflagellates create a feeding current that transports prey particles to the sulcus area, co-occurring with the site of prey capture and engulfment (Hansen and Calado, 1999; Roberts *et al.*, 2011). Dinoflagellates with an anterior

transverse flagellum do not push water in front of the swimming cell; instead, a feeding current directs prey toward the entire anterior part of the dinoflagellate. This is consistent with our observations of prey capture occurring anteriorly in *A. longum*.

For *G. dominans* and *O. marina*, the magnitude of flow provided via the feeding current compares well with earlier observations of clearance rates, at least for large prey, and the feeding current thus presents a satisfactory explanation for observed prey encounter rates. Our clearance rate calculations are based solely on interception feeding that requires physical contact between predator and prey. No remote sensing of the prey, chemical or physical, is assumed. It is clear that many protists (including dinoflagellates) are chemotactic and are able to remain in patches of elevated food concentrations or otherwise advantageous conditions (Spero, 1985; Martel, 2006; Berge *et al.*, 2008). In addition, the ciliate *Mesodinium pulex* has been shown to use the hydromechanical signals to detect its prey, but this is, to our knowledge, the only protist species for which this has so far been shown (Jakobsen *et al.*, 2006). It still remains largely unexplored whether dinoflagellates are able to remotely detect individual prey and thereby increase prey encounter rate. If sensing (chemical or hydromechanical) is indeed directly involved in *G. dominans* and *O. marina* feeding, clearance rates are potentially higher than calculated here. It should be noted, however, that we did not observe remote prey sensing in either species. The clearance estimates are also very sensitive to the predator's swimming speed. In our experiments, both dinoflagellates swam at $\approx 200\text{--}300 \mu\text{m s}^{-1}$, but *O. marina* has been reported to swim as fast as $700 \mu\text{m s}^{-1}$ (Cosson *et al.*, 1988). Finally, our calculated clearance rates assume nonmotile prey; prey motility may increase prey encounter velocity and, hence, clearance rate. Thus, our calculated clearance rates are conservative estimates but suggest a significant role of the feeding current for prey encounter in dinoflagellates. Interception feeding, with its haphazard particle collection, thus appears the strategy in these fast-swimming heterotrophic dinoflagellates. This has direct implications for models of interactions among plankton organisms, including prey encounter rates.

Here we have shown how dinoflagellates manage to capture prey particles without pushing them away, but all other phagocytizing microorganisms similarly need to overcome viscosity to encounter prey. Some resolve to filter feeding, for example, choanoflagellates, some sessile nanoflagellates and ciliates (Sleigh, 1964; Fenchel, 1982, 1986; Fenchel and Patterson, 1986; Pettitt *et al.*, 2002), others are diffusion feeders that depend on prey swimming across the viscous boundary (Fenchel, 1984; Langlois *et al.*, 2009) and others again have developed rather unique methods such as the toxic mucus traps of *Alexandrium pseudogonyaulax* (Blossom *et al.*, 2012). Although interception

feeding may be common among free-swimming flagellates (Fenchel, 1984), fluid dynamics have mostly been studied for sessile forms (Fenchel, 1982; Christensen-Dalsgaard and Fenchel, 2003), and our results are, to our knowledge, the first empirical quantification of the importance of feeding currents in free-swimming interception feeders. Moreover, feeding currents should be present in nearly all phagocytizing microorganisms as they appear a prerequisite for successful particle feeding.

Quick or quiet?

The magnitude of fluid deformation produced by swimming dinoflagellates are comparable to levels that may elicit escape responses in their prey items (Jakobsen, 2001, 2002; Jakobsen *et al.*, 2006). Interestingly though, there were large differences among the dinoflagellates in the magnitude and pattern of fluid deformation created. Some dinoflagellates (here represented by *O. marina* and *G. dominans*) rely on rapid swimming in order to encounter as much prey as possible, and in the process sacrifice hydrodynamic stealth. Thus, they must either rely on nonevasive prey or be able to catch the prey despite evasive actions. Others—here represented by the remaining species—take a slow-swimming approach that allows them to approach their prey unnoticed. The case of *Dinophysis* spp. is particularly interesting, as it feeds solely on the evasive and very fast swimming ciliate *M. rubrum* (Park *et al.*, 2006; Reguera *et al.*, 2012). Nagai *et al.* (2008) described how *Dinophysis fortii* captured *M. rubrum* directly with its peduncle, but also described excreted mucus as an alternative strategy, and prey clump formation, supposedly mediated by an excreted allelochemical, as a third. Alternatively, Hansen *et al.* (2013) described how *Dinophysis* spp. catch *M. rubrum* using capture filaments deployed at a distance, presumably informed by leaked chemical substances. Both lack documentation, however, and one may rightfully ask how the slow dinoflagellate is able to catch the fast and alert ciliate? The threshold deformation rate to elicit an escape response in *M. rubrum* is $\sim 3 \text{ s}^{-1}$ (Jakobsen, 2001; Fenchel and Hansen, 2006) and our observations show that the deformation rate in the feeding current of *D. acuta* does not exceed this threshold, suggesting the dinoflagellate is able to intercept its prey without eliciting its escape. Hence, different feeding strategies emerge, signifying a tradeoff between prey encounter rates and escape responses. The observed differences were related mostly to swimming speeds, and were not tightly coupled with the position of the transverse flagellum.

Increasing nutrient uptake by swimming

Swimming significantly increased the flux of inorganic nutrients to the mixotrophic dinoflagellate *D. acuta*. The observed increase ($\approx 75\%$)

would be equivalent for other substances, for example oxygen, CO_2 and HCO_3^{-1} , ions and infochemicals. This is, to our knowledge, the first attempt to calculate potential fluxes to swimming microorganisms based on empirical observations of their flow fields. Previous work has described theoretically the flux to a sinking sphere, moved only by gravity (Clift *et al.*, 1978; Kjørboe *et al.*, 2001), and to self-propelled uni-flagellated protists (Langlois *et al.*, 2009) and ‘squirmes’ (Magar *et al.*, 2003; Magar and Pedley, 2005). For size and speed similar to that of the dinoflagellate *D. acuta*, the theory of a sinking sphere predicts a Sherwood number of ≈ 1.5 , that of squirmers ≈ 2.0 and of the uni-flagellate between 1.5 and 2.0, depending on the length of the flagellum. The difference owes to the fact that streamlines come much closer in a self-propelled organism than to a translating sphere moved by a body force. This in turn ensures a steep gradient near the cell that enhances the flux. Our result, based on empirical observations of the flow field around a self-propelled dinoflagellate, was in the middle of theoretical estimates, and denotes a significant increase in nutrient uptake because of swimming. Jiang (2011) used computational fluid dynamics to estimate nutrient transport to another mixotrophic protist, the jumping ciliate *M. rubrum*; during its very fast jumps, ≈ 500 body lengths s^{-1} , it may increase nutrient transport by a factor 5.

Large cells are generally poor competitors for inorganic nutrients compared with small ones as diffusion-limited mass-specific nutrient uptake scales inversely with cell radius squared (Kjørboe, 2008). Large-sized diatoms combat diffusion limitation by an inflated-volume strategy (Thingstad *et al.*, 2005): by having a vacuole that efficiently increase the cell size—but not the biomass—and therefore the absolute diffusive transport, they are able to increase the mass-specific nutrient uptake by a factor of 2–5 relative to that of a denser cell of the same biomass. Large-sized dinoflagellates and other mixotrophic motile protists achieve a similar enhancement in nutrient uptake by generating feeding and swimming currents. Swimming and feeding currents also allow dinoflagellates to intercept prey particles, permitting a mixotrophic strategy. This may help explain the evolutionary success of dinoflagellates in the ocean.

Conflict of Interest

The authors declare no conflict of interest.

Acknowledgements

We thank Suzanne Strom for kindly providing the cultures of *A. longum* and *G. dominans*. We also thank Berit M Martensen for calculating nutrient fluxes. The Centre for Ocean Life is a Villum Kahn Rasmussen Center of Excellence funded by the Villum Foundation.

References

- Beardon RN, Magar V. (2010). Simple models of the chemical field around swimming plankton. *J Plankton Res* **32**: 1599–1608.
- Berek VM. (1927). Grundlagen der Tiefenwahrnehmung im Mikroskop, mit einem Anhang über die Bestimmung der obersten Grenze des unvermeidlichen Fehlers einer Messung aus der Häufigkeitsverteilung der zufälligen Maximalfehler. *Sitzungsber ges beförder ges naturwiss Marbg* **62**: 189–223.
- Berge T, Hansen P, Moestrup Ø. (2008). Feeding mechanism, prey specificity and growth in light and dark of the plastidic dinoflagellate *Karlodinium armiger*. *Aquat Microb Ecol* **50**: 279–288.
- Blossom HE, Daugbjerg N, Hansen PJ. (2012). Toxic mucus traps: a novel mechanism that mediates prey uptake in the mixotrophic dinoflagellate *Alexandrium pseudogonyaulax*. *Harmful Algae* **17**: 40–53.
- Christensen-Dalsgaard K, Fenchel T. (2003). Increased filtration efficiency of attached compared to free-swimming flagellates. *Aquat Microb Ecol* **33**: 77–86.
- Clift R, Grace JR, Weber ME. (1978). *Bubbles, Drops and Particles*. Academic Press: New York.
- Cosson J, Cachon M, Cachon J, Cosson M-P. (1988). Swimming behaviour of the unicellular biflagellate *Oxyrrhis marina*: in vivo and in vitro movement of the two flagella. *Biol Cell* **63**: 117–126.
- Drescher K, Dunkel J, Cisneros LH, Ganguly S, Goldstein RE. (2011). Fluid dynamics and noise in bacterial cell-cell and cell-surface scattering. *Proc Natl Acad Sci USA* **108**: 10940–10945.
- Drescher K, Goldstein RE, Michel N, Polin M, Tuval I. (2010). Direct measurement of the flow field around swimming microorganisms. *Phys Rev Lett* **105**: 168101.
- Fenchel T. (1982). Ecology of heterotrophic microflagellates. I. Some important forms and their functional morphology. *Mar Ecol Prog Ser* **8**: 211–223.
- Fenchel T. (1984). Suspended marine bacteria as a food source. In: Fasham M (ed) *Flows of Energy and Materials in Marine Ecosystems*. Plenum Press: New York, pp 301–315.
- Fenchel T. (1986). Protozoan filter feeding. *Prog Protistol* **1**: 65–113.
- Fenchel T. (2001). How dinoflagellates swim. *Protist* **152**: 329–338.
- Fenchel T, Hansen PJ. (2006). Motile behaviour of the bloom-forming ciliate *Mesodinium rubrum*. *Mar Biol Res* **2**: 33–40.
- Fenchel T, Patterson D. (1986). *Percolomonas cosmopolitus* (Ruinen) n.gen., a new type of filter feeding flagellate from marine plankton. *J Mar Biol Assoc UK* **66**: 465–482.
- Fiksen Ø, Follows MJ, Aksnes DL. (2013). Trait-based models of nutrient uptake in microbes extend the Michaelis-Menten framework. *Limnol Oceanogr* **58**: 193–202.
- Flynn KJ, Stoecker DK, Mitra A, Raven JA, Glibert PM, Hansen PJ *et al.* (2013). Misuse of the phytoplankton-zooplankton dichotomy: the need to assign organisms as mixotrophs within plankton functional types. *J Plankton Res* **35**: 3–11.
- Goldstein RE. (2015). Green algae as model organisms for biological fluid dynamics. *Annu Rev Fluid Mech* **47**: 343–375.
- Hansen PJ, Calado AJ. (1999). Phagotrophic mechanisms and prey selection in free-living dinoflagellates. *J Eukaryot Microbiol* **46**: 382–389.
- Hansen PJ, Nielsen LT, Johnson M, Berge T, Flynn KJ. (2013). Acquired phototrophy in *Mesodinium* and *Dinophysis* – a review of cellular organization, prey selectivity, nutrient uptake and bioenergetics. *Harmful Algae* **28**: 126–139.
- Jakobsen H. (2002). Escape of protists in predator-generated feeding currents. *Aquat Microb Ecol* **26**: 271–281.
- Jakobsen H. (2001). Escape response of planktonic protists to fluid mechanical signals. *Mar Ecol Prog Ser* **214**: 67–78.
- Jakobsen H, Everett L, Strom S. (2006). Hydromechanical signaling between the ciliate *Mesodinium pulex* and motile protist prey. *Aquat Microb Ecol* **44**: 197–206.
- Jiang H. (2011). Why does the jumping ciliate *Mesodinium rubrum* possess an equatorially located propulsive ciliary belt? *J Plankton Res* **33**: 998–1011.
- Karp-Boss L, Boss E, Jumars P. (1996). Nutrient fluxes to planktonic osmotrophs in the presence of fluid motion. *Oceanogr Mar Biol* **34**: 71–107.
- Kjørboe T. (2008). *A mechanistic Approach to Plankton Ecology*. Princeton University Press: New Jersey.
- Kjørboe T. (2011). How zooplankton feed: mechanisms, traits and trade-offs. *Biol Rev Camb Philos Soc* **86**: 311–339.
- Kjørboe T, Jiang H, Goncalves RJ, Nielsen LT, Wadhwa N. (2014). Flow disturbances generated by feeding and swimming zooplankton. *Proc Natl Acad Sci USA* **111**: 11738–11743.
- Kjørboe T, Ploug H, Thygesen UH. (2001). Fluid motion and solute distribution around sinking aggregates. I. Small-scale fluxes and heterogeneity of nutrients in the pelagic environment. *Mar Ecol Prog Ser* **211**: 1–13.
- Kjørboe T, Saiz E, Visser A. (1999). Hydrodynamic signal perception in the copepod *Acartia tonsa*. *Mar Ecol Prog Ser* **179**: 97–111.
- Kjørboe T, Visser A. (1999). Predator and prey perception in copepods due to hydromechanical signals. *Mar Ecol Prog Ser* **179**: 81–95.
- Langlois V, Andersen A, Bohr T, Visser A, Fishwick J, Kjørboe T. (2009). Significance of swimming and feeding currents for nutrient uptake in osmotrophic and interception feeding flagellates. *Aquat Microb Ecol* **54**: 35–44.
- Lee KH, Jeong HJ, Yoon EY, Jang SH, Kim HS, Yih W. (2014). Feeding by common heterotrophic dinoflagellates and a ciliate on the red-tide ciliate *Mesodinium rubrum*. *ALGAE* **29**: 153–163.
- Magar V, Goto T, Pedley TJ. (2003). Nutrient uptake by a self-propelled steady squirmer. *Q J Mech Appl Math* **56**: 65–91.
- Magar V, Pedley TJ. (2005). Average nutrient uptake by a self-propelled unsteady squirmer. *J Fluid Mech* **539**: 93.
- Martel CM. (2006). Prey location, recognition and ingestion by the phagotrophic marine dinoflagellate *Oxyrrhis marina*. *J Exp Mar Bio Ecol* **335**: 210–220.
- Munk W, Riley G. (1952). Absorption of nutrients by aquatic plants. *J Mar Res* **11**: 215–240.
- Nagai S, Nitshitani G, Tomaru Y, Sakiyama S, Kamiyama T. (2008). Predation by the toxic dinoflagellate *Dinophysis fortii* on the ciliate *Myrionecta rubra* and observation of sequestration of ciliate chloroplasts. *J Phycol* **44**: 909–922.

- Park M, Kim S, Kim H, Myung G, Kang Y, Yih W (2006). First successful culture of the marine dinoflagellate *Dinophysis acuminata*. *Aquat Microb Ecol* **45**: 101–106.
- Pettitt ME, Orme BAA, Blake JR, Leadbeater BSC. (2002). The hydrodynamics of filter feeding in choanoflagellates. *Eur J Protistol* **38**: 313–332.
- Reguera B, Velo-Suárez L, Raine R, Park MG. (2012). Harmful dinophysis species: a review. *Harmful Algae* **14**: 87–106.
- Roberts EC, Wootton EC, Davidson K, Jeong HJ, Lowe CD, Montagnes DJS. (2011). Feeding in the dinoflagellate *Oxyrrhis marina*: linking behaviour with mechanisms. *J Plankton Res* **33**: 603–614.
- Sleigh MA. (1964). Flagellar movement of sessile flagellates *Actinomonas*, *Codonosiga*, *Monas*, and *Poteriodendron*. *Q J Microsc Sci* **105**: 405–415.
- Spero H. (1985). Chemosensory capabilities in the phagotrophic dinoflagellate *Gymnodinium-fungiforme*. *J Phycol* **21**: 181–184.
- Stoecker DK. (1998). Conceptual models of mixotrophy in planktonic protists and some ecological and evolutionary implications. *Eur J Protistol* **34**: 281–290.
- Stoecker DK. (1999). Mixotrophy among dinoflagellates. *J Eukaryot Microbiol* **46**: 397–401.
- Thingstad TF, Øvreås L, Egge JK, Løvdal T, Heldal M. (2005). Use of non-limiting substrates to increase size; a generic strategy to simultaneously optimize uptake and minimize predation in pelagic osmotrophs? *Ecol Lett* **8**: 675–682.
- Yoo Y, Jeong H, Kang N, Kim J, Kim T, Yoon E. (2010). Ecology of *Gymnodinium aureolum*. II. Predation by common heterotrophic dinoflagellates and a ciliate. *Aquat Microb Ecol* **59**: 257–272.

Supplementary Information accompanies this paper on The ISME Journal website (<http://www.nature.com/ismej>)